Overview of recent physics results from NSTX

S.M. Kaye[1], T. Abrams[1], J-W. Ahn[2], J. Allain[3], R. Andre[1], D. Andruczyk[3], R. Barchfeld[4], D. Battaglia[1], A. Bhattacharjee[1], F. Bedoya[3], R. Bell[1], E. Belova[1], J. Berkery[5], L. Berry[2], N. Bertelli[1], R. Betti[6], P. Beiersdorfer[7], J. Bialek[5], R. Bilato[8], J. Boedo[9], P. Bonoli[10], A. Boozer[5], A. Bortolon[11], D. Boyle[1], D. Brennan[12], J. Breslau[1], J. Brooks[13], R. Buttery[14], A. Capece[1], J. Canik[2], C. S. Chang[1], N. Crocker[15], D. Darrow[1], W. Davis[1], L. Delgado- Aparicio[1], A. Diallo[1], D. D'Ippolito[16], C. Domier[4], F. Ebrahimi[12], S. Ethier[1], T. Evans[14], N Ferraro[14], J. Ferron[14], M. Finkenthal[17], R. Fonck[18], E. Fredrickson[1], G.Y. Fu[1], D. Gates[1], S. Gerhardt[1], A. Glasser[19], N. Gorelenkov[1], M. Gorelenkova[1], I. Goumiri[12], T. Gray[2], D. Green[2], W. Guttenfelder[1], R. Harvey[20], A. Hassanein[13], W. Heidbrink[21], Y. Hirooka[22], E.B. Hooper[7], J. Hosea[1], D. Humphreys[14], E.F. Jaeger[23], T. Jarboe[19], S. Jardin[1], M.A. Jaworski[1], R. Kaita[1], C. Kessel[1], K. Kim[1], B. Koel[12], E. Kolemen[1], G. Kramer[1], S. Ku[1], S. Kubota[15], R.J. La Haye[14], L. Lao[14], B. LeBlanc[1], F. Levinton[24], D. Liu[21], J. Lore[12], M. Lucia[3], N. Luhmann Jr.[15], R. Maingi[1], R. Majeski[1], D. Mansfield[1], R. Maqueda[24], G. McKee[18], S. Medley[1], E. Meier[7], J. Menard[1], D. Mueller[1], T. Munsat[25], C. Muscatello[4], J. Myra[16], B. Nelson[19], J. Nichols[1], M. Ono[1], T. Osborne[14], J.-K. Park[1], Y. Park[5], W. Peebles[15], R. Perkins[1], C. Phillips[1], M. Podesta[1], F. Poli[1], R. Raman[19], Y. Ren[1], J. Roszell[12], C. Rowley[12], D. Russell[16], D. Ruzic[3], P. Ryan[2], S.A. Sabbagh[5], E. Schuster[26], F. Scotti[7], Y. Sechrest[25], K. Shaing[18], T. Sizyuk[13], V. Sizyuk[13], C. Skinner[1], D. Smith[18], P. Snyder[14], W. Solomon[12], C. Sovenic[18], V. Soukhanovskii[7], E. Startsev[1], D. Stotler[1], B. Stratton[1], D. Stutman[17], H. Takahashi[1], G. Taylor[1], C. Taylor[13], K. Tritz[17], M. Walker[14], W. Wang[1], Z. Wang[1], R. White[1], J.R. Wilson[1], B. Wirth[11], J. Wright[10], X. Yuan[1], H. Yuh[24], L. Zakharov[1], G. Zimmer[1], S.J. Zweben[1]

[1] Princeton Plasma Physics Laboratory, Princeton, NJ, USA
[2] Oak Ridge National Laboratory, Oak Ridge, TN, USA
[3] University of Illinois at Urbana-Champaign, Urbana, IL, USA
[4] University of California at Davis, Davis, CA, USA
[5] Columbia University, New York, NY, USA
[6] University of Rochester, Rochester, NY, USA
[7] Lawrence Livermore National Laboratory, Livermore, CA, USA
[8] IPP, Garching, Germany
[9] University of California at San Diego, San Diego, CA, USA
[10] Massachusetts Institute of Technology, Cambridge, MA, USA
[11] University of Tennessee, Knoxville, TN, USA
[12] Princeton University, Princeton, NJ USA
[13] Purdue University, Purdue, IA, USA
[14] General Atomics, San Diego, CA, USA
[15] University of California at Los Angeles, Los Angeles, CA, USA
[16] Lodestar Research Corporation, Boulder, CO, USA
[17] Johns Hopkins University, Baltimore, MD, USA
[18] University of Wisconsin, Madison, WI, USA
[19] University of Washington, Seattle, WA, USA
[20] CompX, Del Mar, CA, USA

[21] University of California at Irvine, Irvine, CA, USA
[22] National Institute for Fusion Science, Oroshi, Toki, Gifu, Japan
[23] XCEL, Oak Ridge, TN, USA
[24] Nova Photonics, Inc., Princeton, NJ, USA
[25] University of Colorado at Boulder, Boulder, CO, USA
[26] Lehigh University, Bethlehem, PA, USA

e-mail contact of main author: skaye@pppl.gov

Abstract

NSTX is currently being upgraded to operate at twice the toroidal field and plasma current (up to 1 T and 2 MA), with a second, more tangentially aimed neutral beam for current and rotation control, allowing for pulse lengths up to 5 s. Recent NSTX physics analyses have addressed topics that will allow NSTX-U to achieve the research goals critical to a Fusion Nuclear Science Facility. These goals include producing stable, 100% non-inductive operation, assessing Plasma Material Interface (PMI) solutions to handle the high heat loads expected in the next-step devices, and accessing low collisionality and high beta. Upgrade construction is moving on schedule with initial operation of NSTX-U planned for early 2015.

1. Introduction

Recent analysis of data from the National Spherical Torus Experiment (NSTX) has focused on topics critical to the development of the research plan and achievement of physics goals for the NSTX-Upgrade[1]. NSTX (R/a=0.85/0.65 m, κ=1.8-2.4, δ=0.3-0.8, I_p up to 1.5 MA, B_T up to 0.55 T) ceased operation in Oct. 2010 in order to begin Upgrade construction activities. NSTX-U has three primary research goals:

1. **To advance the Spherical Torus (ST) concept for a Fusion Nuclear Science Facility.** Demonstrate 100% non-inductive sustainment, and develop non-inductive start-up and ramp-up techniques for an FNSF[2] with a small, or no, solenoid.

2. **To develop solutions for the plasma-material interface (PMI).** Mitigate high heat fluxes (up to five times greater than in NSTX), and assess high-Z and liquid lithium plasma facing components (PFC).

3. **To explore unique ST parameter regimes to advance predictive capability for ITER and beyond.** Access reduced collisionality and high-β (β_n~6) at enhanced confinement, stability and non-inductive current drive.

The increased capabilities of NSTX-U (R/a = 0.95/0.55 m, κ~2.8) will facilitate the research necessary to achieve these goals. The major capabilities include a factor of ~two increase in both plasma current I_p and toroidal magnetic field B_T to 2 MA and 1 T respectively, and an additional off-axis neutral beam that will double the available input beam power to 12 MW. The first two enhancements will allow for high-β operation at almost an order-of-magnitude lower collisionality[3], and the second neutral beam, coupled with up to 6 MW of High Harmonic Fast Wave (HHFW) power, will provide means to vary the q- and rotation profile,

and will provide significant non-inductive current drive directly or indirectly. This, along with advanced control algorithms, will enable NSTX-U to sustain stable, high performance discharges near steady-state conditions for pulse lengths up to 5 s.

2. Advance the Spherical Torus (ST) concept for a Fusion Nuclear Science Facility.

An envisioned strategy for non-inductive operation in NSTX-U employs Co-axial Helicity Injection (CHI) for plasma initiation, ECH to heat the plasma from an initial temperature of 10's of eV to up to several hundred 100 eV, and HHFW to heat the plasma further to the 1 to 3 keV level. Then, HHFW and/or NBI current drive would be used to ramp the plasma current up to full current at which time NBCD and bootstrap current would be utilized to sustain the full current non-inductively.

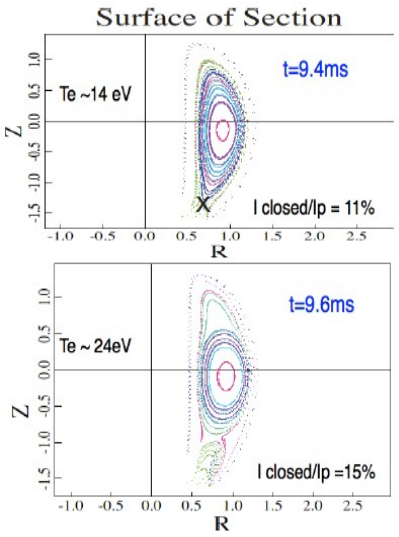

Figure 1 Poincare plots soon after flux closure for (a) 14 eV and (b) 24 eV.

CHI has been successfully used for plasma formation in NSTX with currents up to 200 kA with coupling to inductive ramp-up[4]. The underlying physics of CHI startup has been studied with resistive MHD simulations using the NIMROD[5] code in 2D[6]. The simulations indicate that the magnetic diffusivity strongly controls flux closure, with no flux closure at high diffusivity corresponding to temperatures lower than those measured in the experiment (T_e~1 eV), but flux closure occurs as T_e increases towards the experimental values (10 to 25 eV). Field line tracing was used to confirm the formation of the X-point and flux closure, as is shown in Figure **1** for two temperatures, T_e=14 and 24 eV. The simulations have also shown that the X-point formation may be a Sweet-Parker type reconnection.

Full wave simulations using the AORSA code[7] have shown that the wave electric field in the SOL is small at low density, when the FW cutoff is in front of the antenna, but becomes quite large at high density when the FW cutoff "opens up"[8]. When the cutoff is in front of the antenna, the waves are evanescent, but they can propagate when the cutoff opens at high density. Using an artificial "collisional" damping in AORSA, the fraction of RF power lost to the SOL as a function of density in front of the antenna for two different toroidal wavenumbers n_ϕ is shown in Figure **2**. In the figure, the vertical lines reflect the density at which the FW cutoff "opens up" for the respective wavenumbers. The figure shows the rapid increase in lost power as the wave transitions from the evanescent (low n_{ant})

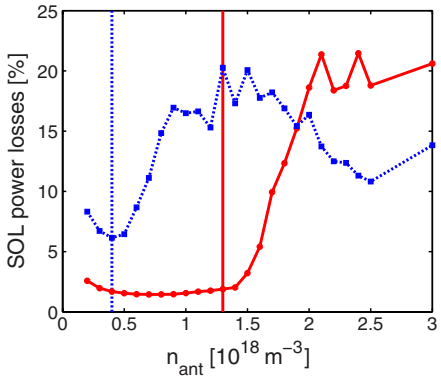

Figure 2 Fraction of power lost to the SOL as a function of density in front of the antenna for n_ϕ=-21 (solid red) and n_ϕ=-12 (dashed blue).

to propagating (high n_{ant}) regimes respectively. These calculations have been extended to NSTX-U, and the results indicate a wider SOL density range with low SOL power losses.

Time dependent simulations with the free boundary equilibrium solver ISOLVER in TRANSP have begun in order to develop fully non-inductive NSTX-U discharge scenarios. The simulations indicate that 1 MW of EC heating can rapidly heat plasmas generated by CHI. T_e increases from 10-20 eV, typical of CHI plasmas, to about 1 keV in 30 ms. Up to 4 MW of HHFW is then used in conjunction with EC to further heat the plasma and to drive current to facilitate NBI with minimal fast ion losses. The combined EC/HHFW heating can delay the decrease of the CHI generated current and sustain a non-inductive current of 350 kA. With 10 MW of NBI distributed over the two beamlines, the simulation shows that the current can be ramped up non-inductively to 900 kA in 2.5 s. With the density between 60 and 90% of the Greenwald limit and $H_{98y,2}$~1.0 to 1.2, the total current is sustained with a bootstrap contribution between 40 and 60% (Figure **3**).

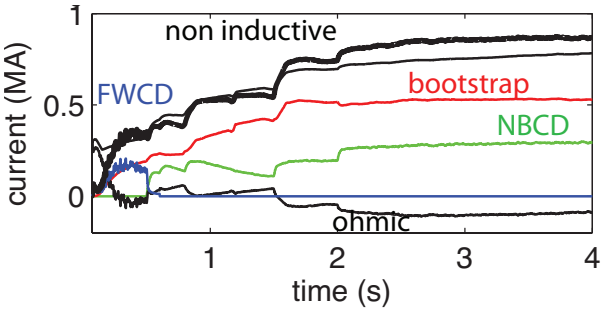

Figure 3 Fully non-inductive current scenario for NSTX-U as computed by TRANSP with the ISOLVER free boundary equilibrium solver.

One requirement for stable operation is the ability to control the Resistive Wall Mode (RWM)[9,10]. Recent work on RWMs, including calculations with the MISK code[11,12] has given a complex picture in which stability is controlled not only by collisional dissipation, but also by kinetic resonances and the plasma rotation profile[13]. This is shown in Figure **4** where the Resonant Field Amplification (RFA) amplitude measured by MHD spectroscopy is plotted as a function of the average plasma ExB rotation frequency for an NSTX H-mode discharge. There is clearly an optimal rotation profile for stable operation (minimum RFA amplitude), and at the corresponding value of $<\omega_E>$ the plasma is on-resonance with the precession drift.

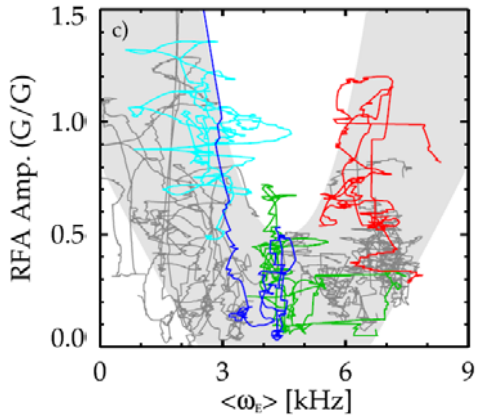

Figure 4 n=1 RFA amplitude as a function of average plasma rotation frequency.

In order to control the plasma rotation, a coupled 1D toroidal rotation model and controller is being developed in order to capture and sustain a favorable plasma rotation profile. In this algorithm, the Neoclassical Toroidal Viscosity (NTV)[14] and NB torque are used as actuators for the controller design. The NTV torque is provided by magnetic perturbations from midplane coils. The NB torque is calculated in the NUBEAM code in TRANSP. The control algorithm is solved and advanced in TRANSP. An example of the first use of this technique is shown in Figure **5** which shows the NTV and NBI torque (top panels) and plasma rotation evolution at two rotation setpoints from the rotation feedback control algorithm. In

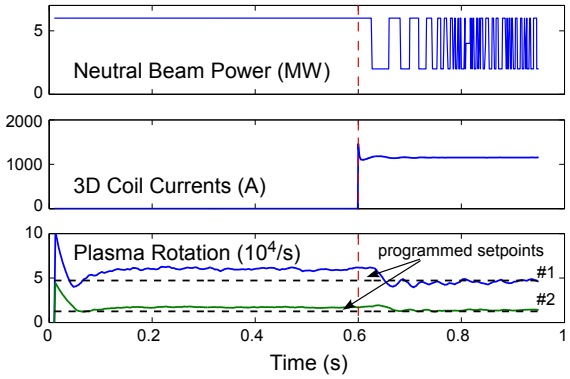

Figure 5 NBI and NTV actuators (top panels) and evolution of plasma rotation vs programmed setpoints using rotation control algorithm.

this example, the NTV was produced by n=3 fields from the midplane MP coils. Using the combined NTV and NB torques, the rotation reaches its target in approximately 20 ms, much shorter that the momentum confinement time of ~150 ms.

Understanding the underlying physics of Neoclassical Toroidal Viscosity (NTV) will allow for more confident use in predictions to future devices. Several recent efforts have extended early experimental work on NTV[43]. In one approach[44], the POCA (Particle Orbit Code for Anisotropic Pressure) code was developed to follow guiding center orbits of particles for precisely calculating δf, the perturbed distribution function, in a non-axisymmetric ideal magnetic field equilibrium determined by IPEC[45]. POCA simulations show the importance of collisionality and particle resonances with the toroidal rotation, similar to that found for RWMs. A comparison of NTV damping rate calculated by POCA with the measured dL/dt from changes in the momentum profile is shown in Figure **6** for an n=3 experiment. As can be seen, the NTV damping rate magnitudes agree roughly in the ψ_n=0.6-0.8 region, although the location of the NTV peak is shifted inward in the POCA calculation, and POCA underestimates the NTV inside of ψ_n=0.5.

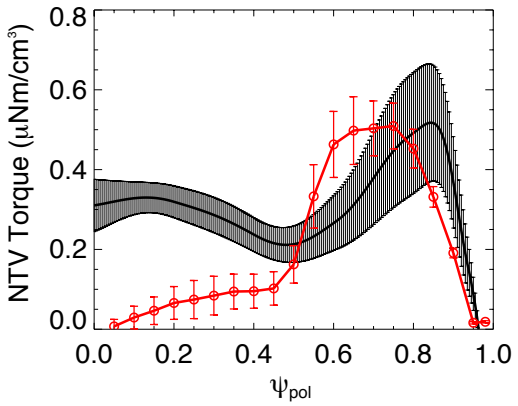

Figure 6 Experimental NTV torque (black) and that calculated from POCA (red).

Another approach to determining the NTV computes the δ**B** fully in 3D, and uses the Shaing formulation of T_{NTV} valid for all collisionality regimes and the superbanana-plateau regime for both ions and electrons as implemented in the NTVTOK code[46]. The calculation includes the effect of the flux surface displacement. Results from the code for an applied n=3 configuration in NSTX are shown in Figure **7**. The calculated T_{NTV} exhibits large radial variations that are not observed experimentally. The calculated radial displacements are smaller than either the ion banana or gyro radii, suggesting finite orbit effects will spatially average T_{NTV}. The red curve is the calculated T_{NTV} averaged over the banana width, and this

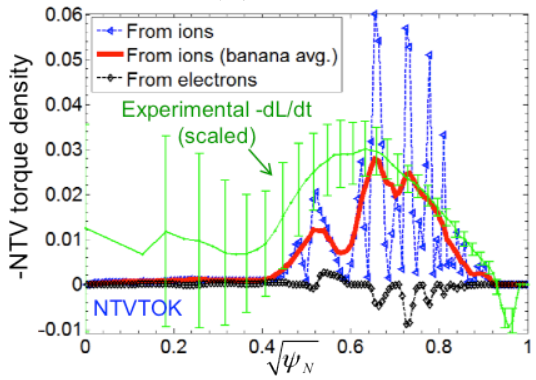

Figure 7 Experimental NTV torque scaled by a factor of ~2 (green) and that calculated from NTVTOK (red).

closely matches the scaled (~2x) experimental dL/dt in the outer region of the plasma where the NTV is the strongest. In this outer region, the flux surface-averaged δ**B** calculated by NTVTOK compares favorably with that computed by M3D-C[1], which includes a resistive plasma response model.

Neutral beam current drive will be used during the discharge sustainment phase to aid the achievement of 100% non-inductive operation. It is, however, important to understand the physics processes that can affect the fast ion distribution in order to develop scenarios to achieve the NSTX-U research goals and to address the performance of future fusion plasma experiments such as ITER. Figure **8** is an existence plot of types of Alfvén activity seen in NSTX. TAE avalanches and other Energetic Particle Modes are observed at low and medium density, while EPMs and quiescent plasmas are seen at higher densities. The figure also shows that the NSTX-U operational space (gray shaded region) overlaps those envisioned for both ITER and an ST-FNSF. The TAE avalanches and EPMs can result in up to a 35% drop in the neutron rate, which has been determined to come primarily from energy loss and spatial redistribution[15].

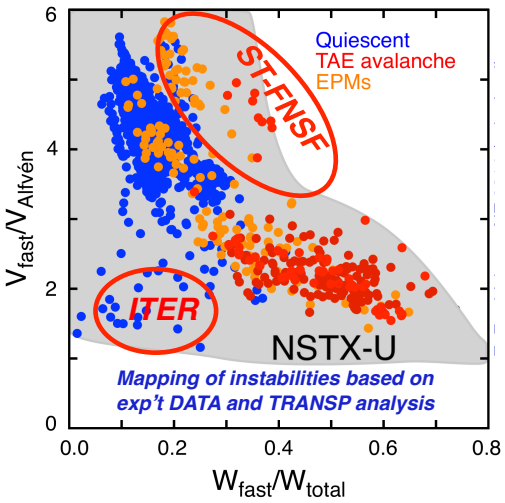

Figure 8 Existence space of various types of Alfvén activity in NSTX.

Recent analysis and theory have also revealed complex relationships between different instabilities. High frequency (1.4 to 2 MHz) Compressional Alfvén Eigenmodes (CAE) exhibit bursting whose frequency is regulated by kink modes in the 2 to 30 kHz frequency range[16] in a predator-prey relation, where the fast ion beta takes the role of the prey, increasing linearly in the absence of mode-induced losses, and the CAE mode amplitude plays the role of the predator, causing fast ion redistribution/loss.

In ST plasmas with weakly reversed magnetic shear and q_{min} slightly above 1, stability calculations[17] indicate that a non-resonant kink modes (NRK) exist. For higher q_{min} and fast particle fraction, higher frequency, beam-driven fishbone modes (EPM) are destabilized. Linear and nonlinear simulations using the global kinetic/MHD hybrid M3D-K code[18] indicate that both the NRK and the fishbone modes significantly affect the fast ion distribution, reducing the fast ion density in the central region of the plasma. The results from these linear and non-linear M3D-K calculations will be used to identify regimes for stable operation in NSTX-U.

The excitation of high frequency Global and Compressional Alfvén modes has been studied for an NSTX H-mode discharge using the hybrid-MHD non-linear HYM code[19]. Results from HYM indicated that unstable CAE modes strongly couple to kinetic Alfvén waves (KAW) on the high field side of the torus, as is seen by the perturbed field structures due to the CAE and KAW modes shown in Figure **9**. The resonance with the KAW is located at the edge of the CAE potential well, just inside the outer edge of the beam ion density profile.

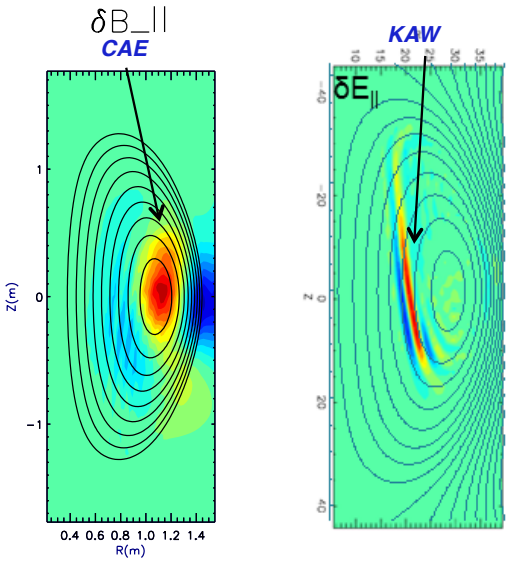

Figure 9 Contour plots of magnetic field perturbation for CAE (left) and electric field contours for KAW (right).

This coupling provides an energy channeling mechanism for beam energy, with a resulting transport of quasi-linear energy flux away from the CAE location at the magnetic axis to the KAW resonance location off-axis. Estimates indicate that up to 0.4 MW of power can be channeled out of the core, which could have a direct effect on the temperature profiles, with changes calculated to be up to several hundred eV. This is one possible explanation for the lack of significant heating of the central T_e observed with increasing beam power with CAE/GAE activity present[20].

Alfvén Eigenmodes and fast ion populations can also be impacted significantly by the application of external 3D fields. Magnetic measurements of energetic ion-driven high frequency bursting CAE/GAE modes have shown that applying even a small δB/B~1% at the plasma edge can lead to a reduction in mode amplitude, an increase in bursting frequency and a smaller frequency chirp[21]. The change in mode characteristics is accompanied by a drop in neutron rate on a time scale that suggests a direct role of the fast ions, and this is borne out by calculations using the SPIRAL[22] code to track the energetic particle distribution in the presence of 3D fields and a resistive plasma response calculated by the M3D-C^1 code[23]. Figure 10 shows the change in fast ion distribution function under the above conditions, indicating a depletion of fast ions for $0.8<v_{||}/v<0.6$ and E>70 keV, precisely at the location of an n=8 ~0.5 MHz GAE resonance. Simulations further suggest a 10 to 20% reduction in dF_{fast}/dv_{perp}, the main driving term.

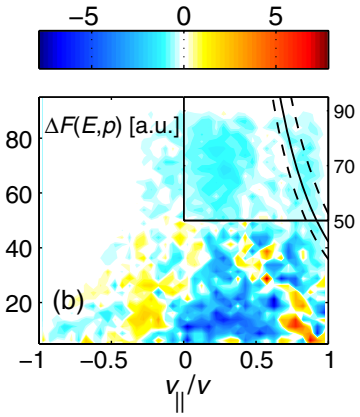

Figure 10 Change in fast ion distribution in plasma core after application of 3D fields.

3. Develop solutions for the plasma-material interface (PMI)

The application of pre-discharge lithium in NSTX has been shown to have beneficial effects for plasma confinement, pedestal structure and ELM suppression[24-27]. Recent analysis on this topic has focused on a dataset covering a wide, contiguous, range of pre-discharge lithium deposition amounts that can address discharge performance and pedestal evolution during and after ELM suppression[28]. With increasing Li deposition, the density pedestal shifted and widened continuously even after ELMs were suppressed. No change was seen in the temperature pedestal location or width. The microinstability properties of the plasma edge due to application of lithium was studied through linear gyrokinetic calculations using the GS2 code[29]. For a discharge without the application of lithium, the calculations showed

that microtearing modes are dominant at the top of the pedestal. With lithium, the increase in the density gradient at that location stabilizes the microtearing mode, and modes with characteristics like those of the TEM became dominant. ETG modes were found to be unstable just inside the separatrix both with and without lithium, suggesting that ETG may play a role in limiting the electron temperature gradient in this region. At mid-pedestal, a hybrid TEM/KBM mode was found to be dominant with and without lithium.

Experiments on NSTX found that both high amounts of lithium wall application to PFCs and increasing plasma current can cause a strong contraction of the SOL heat flux width at the midplane[30]. The XGC1[31] gyrokinetic code was used to study the mechanisms regulating the midplane heat flux width. Preliminary results, assuming a collisionless SOL plasma, indicate that neoclassical processes are primarily responsible for setting the width, given by the banana width ~$1/I_p$. Future work will extend these calculations to finite collisionality and recycling to determine their effect on the predicted SOL heat flux widths.

One potential method to modify the heat flux width is through controlled ELMs. Results from NSTX, however, show that under certain circumstances the heat flux footprint during large ELMs could contract by up to 50%, exacerbating the heat flux challenge. Analysis of this data indicates that the heat flux profile broadening or narrowing (as reflected by the wetted area) is directly correlated with the number of filamentary striations measured in the ELM heat flux profile, as is seen in Figure 11. The striations in the heat flux profile represent ELM filaments and, therefore, could be related to the toroidal mode number of the ELMs before expulsion of the filaments. The typical range of toroidal mode numbers associated with ELM in NSTX is between one and five[27]. The implications of this result suggest that it will be important to identify scenarios that move the projected operating points up to higher-n stability limits for ITER and FNSF.

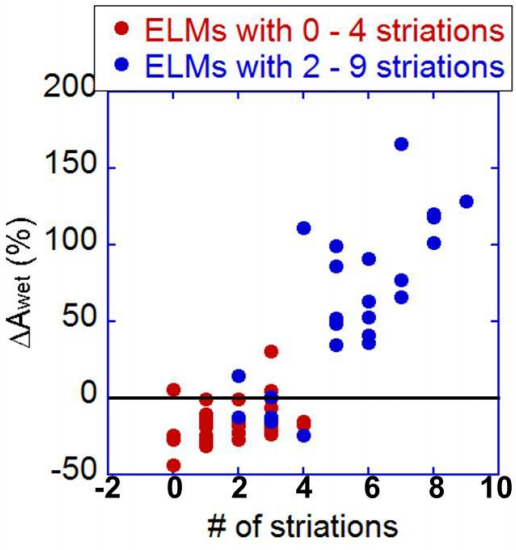

Figure 11 Change in divertor heat flux wetted area as a function of the number of ELM striations

As lithium wall conditioning will be the preferred technique in NSTX-U, with eventual plans to test liquid lithium modules[32], studies have been conducted both in NSTX and in the laboratory to understand lithium-substrate interactions and the effect on both the deposited Li as well as on the substrates. Experiments in NSTX simultaneously addressed lithium sputtering from graphite tiles as well as from both heated and unheated liquid lithium divertor (LLD) modules[33]. Accumulation of carbon impurities was routinely observed in the core of ELM-free lithium-conditioned discharges in NSTX, but despite even large Li deposition, Li concentrations in the plasma core were less than 1% of that of carbon[34].

Sputtering yields of Li from the various surfaces in the NSTX divertor were determined from impurity influx and incident ion flux measurements, in a comparison of discharges with heated and unheated LLD modules[35]. The results indicated that sputtering was enhanced by the higher temperatures on the heated LLD modules. No difference was observed on graphite and on the LLD plate that was unheated, while an enhancement of a factor of 1.5 to 2 was seen over the heated modules when their temperature was above the lithium melting point. The inferred Li sputtering yields were calculated to be ~5% for the unheated LLD modules and above 10% for the heated ones. The core penetration factors for lithium divertor sources inferred from the measured divertor influxes were up to two orders of magnitude lower than those for carbon. This difference, which helps explain the low core accumulation of lithium relative to carbon, can be due to a stronger lithium divertor retention resulting from prompt re-deposition effects as well as from the differences in classical parallel SOL transport shown by UEDGE simulations.

Test stand studies of lithium on metal substrates were carried out on the MAGNUM-PSI linear device at DIFFER[36] in support of the NSTX-U plans to install a row of high-Z (either TZM molybdenum or tungsten) tiles in the lower outboard divertor. For NSTX-related experiments, a lithium evaporator was installed on MAGNUM-PSI. Lithium was deposited onto a substrate material, and then high power discharges were performed, which resulted in surface temperatures up to 1300 C. During the course of exposures, two regimes were found: (1) an intense cloud of lithium emission was formed directly in front of the target, persisting for 3 to 4 sec, and this transitioned into (2) a less intense, more diffuse emission pattern. This intense lithium vapor cloud, which resulted in a reduction of current to the target, will be pursued as a possible divertor heat flux mitigation technique.

Recent surface science experiments conducted at the Princeton Plasma Physics Laboratory have used X-ray photoelectron spectroscopy and temperature programmed desorption to understand the mechanisms for D retention in Li coatings on Mo substrates. The study shows that D is retained as LiD in metallic Li films. However, when oxygen is present in the film, either by diffusion from the subsurface at high temperature or as a contaminant during the deposition process, Li oxides are formed that retain D as LiOD. Experiments indicate that LiD is more thermally stable than LiOD, which decomposes to liberate D_2 gas and D_2O at temperatures 100 K lower than the LiD decomposition temperature. This highlights the importance of maintaining a metallic Li layer as the increased power loading expected in NSTX-U will reach elevated PFC temperatures during the course of a high-power discharge.

4. Explore unique ST parameter regimes to advance predictive capability for ITER and beyond

NSTX/NSTX-U operation at high ρ_i/a (low B_T), low ν_e^*, high beta (β_n up to 6) and low aspect ratio provides a unique parameter regime giving high leverage for validating existing theory as well as for developing ST-specific frameworks. This will, in turn, lead to higher confidence predictions for devices at all aspect ratio. This section will focus on aspects of thermal and fast ion transport and stability that have provided the basis for detailed comparisons to theory and theory development.

The unique features of ST operation mentioned above result in regimes that are distinct from those of conventional aspect ratio tokamaks. In particular, because of the strong toroidal rotation, large ρ_i/a and strong toroidicity and shaping, it is crucial, while highly challenging, to use global gyrokinetic simulations to address turbulence and transport physics. Nonlinear global gyrokinetic simulations of an NSTX L-mode plasma using the GTS code[37] have shown that a drift wave Kelvin-Helmholtz mode can be destabilized by strong toroidal rotation shear. This shear flow mode is characterized by finite $k_{||}$ and broader k_θ than the ITG mode, which is also found to be present in the L-mode. However, even at the reduced level, the remaining low-k fluctuations, while contributing weakly to the observed highly anomalous electron thermal transport, can produce a significant ion thermal transport relevant to the experimental level in the outer core region. Figure **12** shows the comparison of the experimentally inferred electron (left) and ion (right) thermal diffusivities along with the values predicted by GTS. For the ions, the inferred and predicted profiles are within a factor of two in the outer core.

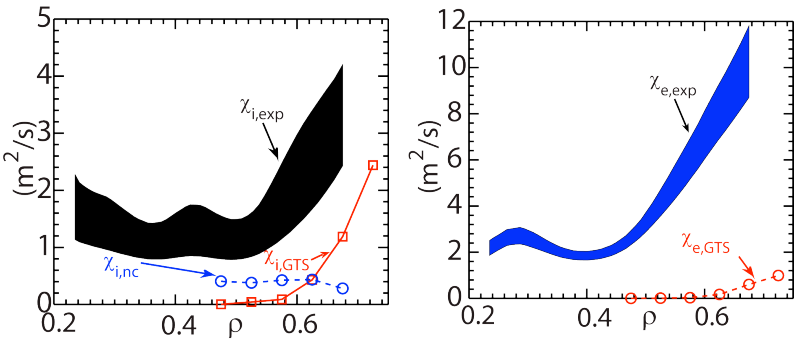

Figure 12 Comparison of experimental and GTS predicted thermal diffusivity for ions (left panel) and electrons (right panel).

Representative H-mode discharges were studied in detail as a basis for a time-evolving prediction of the electron temperature profile using an appropriate reduced transport model. The Rebut-Lallia-Watkins (RLW) electron thermal diffusivity model, which is based on microtearing-induced transport[38,39] was used to predict the time-evolving electron temperature across most of the profile. The results indicate that RLW predicts T_e reasonably well for times and locations where microtearing was determined to be important, but not well when microtearing was predicted to be subdominant[40]. This is shown in Figure **13**, which is a comparison of the linear growth rates (top panels) and predicted and measured T_e profiles (bottom panels) at representative times for two discharges at low and high collisionality respectively. For the low ν_e^* (left panels), the dominant microinstabilities have ballooning parity, and are identified as a hybrid TEM/KBM. For this discharge, the RLW model does a poor job of predicting the T_e profile. However, for the higher ν_e^* discharge (right panel), where microtearing is calculated to be dominant, RLW does an excellent job in matching the T_e profile in the region from x=0.2 to 0.8.

Highly non-linear electron thermal transport was observed in a set of RF-only heated L-mode plasmas. It was observed that electron-scale turbulence spectral power, as measured by a high-k collective microwave scattering system at r/a~0.6, was reduced significantly following the cessation of RF heating. While the drop in turbulence was on a fast time scale (0.5 to 1 ms), there was virtually no change in the local equilibrium quantities that would be expected to drive the turbulence (e.g., a/L_{Te}, a/L_{Ti}, a/L_{ne}) on this time scale; the changes in these quantities occurred on confinement time scales (e.g., tens of ms). Linear stability analysis has shown that both ion- and electron-scale microinstabilities are unstable in the high-k measurement region, and that, linearly, the profiles are well above marginal stability. Non-linear calculations indicate that the turbulence and transport changes are the result of non-local effects.

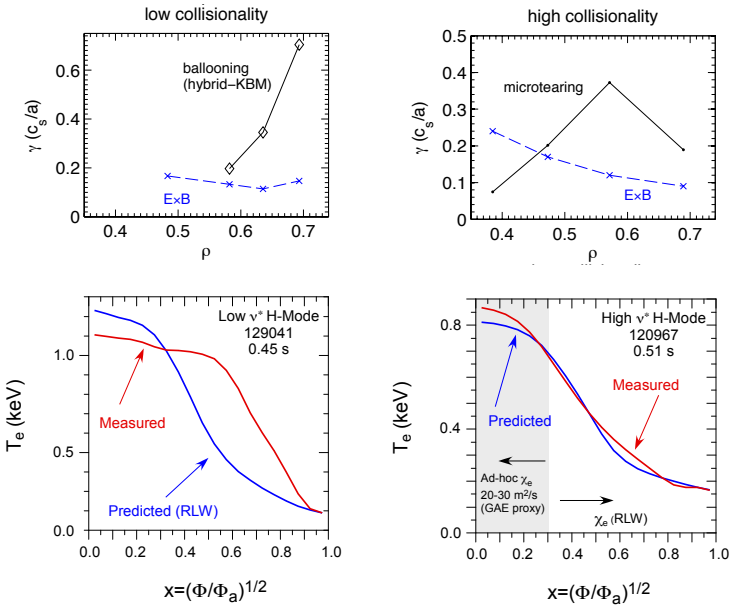

Figure 13 Linear growth rates (top) and measured vs predicted T_e using the RLW model (bottom) for a low (right) and high (left collisionality H-mode discharge.

A model has been developed to predict the effects that some of the AE scenarios discussed in Sec. 2 may have on the fast ion distribution and thus NB current drive. The model uses a probability distribution function that produces changes in a particle's phase space coordinates through 'kicks', due to a resonant interaction with a given set of instabilities[41]. The size of the phase space kicks are taken to scale linearly with mode amplitude, which can be computed from an observable quantity such as neutron rate and the ideal mode structure as computed by NOVA[42]. The model has been implemented in the standalone NUBEAM code, and initial benchmarks indicate good agreement between calculated and measured neutron rates in an NSTX discharge with bursting TAE activity.

Modes driven unstable above the pressure-driven, no wall kink limit can constrain fusion performance. One much studied mode, the Resistive Wall Mode (RWM), has relatively slow growth rates ($\gamma\tau_{wall}$~1), and, as previously discussed, can be stabilized by kinetic effects and passive and active feedback control. In plasmas with stable RWM, and Ideal Wall Mode (IWM) can be driven unstable near the ideal wall limit. The IWM has much higher frequencies and growth rates than the RWM. Recent MARS-K linear calculations have shown that both rotation and kinetic effects can modify IWM stability limits.

Physics research operations on NSTX-U are planned to begin in Spring 2015.

Acknowledgement

This research was supported by US DOE contract DE-AC02-76CH04666.

References

[1] Menard, J. S. Gerhardt, M. Bell et al., Nucl. Fusion **52** (2012) 083015.
[2] Menard, J., L. Bromberg, T. Brown et al., Nucl. Fusion **51** (2011) 103014.
[3] Gerhardt, S.P., R. Andre, J. Menard et al., Nucl. Fusion **52** (2012) 083020.
[4] Raman, R., D. Mueller, T. Jarboe et al., Phys. Plasmas **18** (2011) 092504.
[5] Sovenic, C.R., A.H. Glasser, T.A. Gianakon et al., J. Comput. Phys. **195** (2004) 355.
[6] Hooper, E.B., C.R. Sovinec, R. Raman et al., Phys. Plasmas **20** (2013) 092510.
[7] Jaeger, E.F. et al., Phys. Plasmas **8** (2001) 1573.
[8] Bertell, N., E.F. Jaeger, J.C. Hosea, et al., Nucl. Fusion **54** (2014) 083004.
[9] Kaye, S.M., G.L. Jahns, A.W. Morris et al., Nucl. Fusion **28** (1988) 1963.
[10] Bondeson A. and D. Ward, Phys. Rev. Lett. **72** (1994) 2709.
[11] Hu, B. and R. Betti, Phys. Rev. Lett. **93** (2004) 105002.
[12] Berkery, J.W., Y.Q. Liu, Z.R. Wang et al., Phys. Plasmas **21** (2014) 052505.
[13] Berkery, J.W. et al. Phys. Plasmas **17** (2010) 082504.
[14] Shaing, K.C., and J. D. Callen, Phys. Fluids **26** (1983) 3315.
[15] Fredrickson, E.D., N.A. Crocker, D.S. Darrow et al., Nucl. Fusion **53** (2013) 013006.
[16] Fredrickson, E.D., N.N. Gorelenkov, M. Podesta et al., Phys. Plasmas **20** (2013) 042112.
[17] Wang, F., G.Y. Fu, J.A. Breslau et al., Phys. Plasmas **20** (2013) 072506.
[18] Park, W., E.V. Belova, G.Y. Fu et al., Phys. Plasmas **6** (1999) 1796.
[19] Belova, E.V. et al., Phys. Plasmas **7** 4996 2000; **10** (2003) 3240.
[20] Stutman, D. et al., Phys. Rev. Lett. **102** (2009) 115002.
[21] Bortolon, A., W.W. Heidbrink, G.J. Kramer et al., Phys. Rev. Lett. **110** (2013) 265008.
[22] Kramer, G.J., R.V. Budny, A. Bortolon et al., Plasma Phys. Cont. Fusion **55** (2013) 025053.
[23] Ferrarro, N.M. and S.C. Jardin, J. Comput. Phys. **228** (2009) 7742.
[24] Mansfield, D.K. et al., J. Nucl. Mat. **390-391** (2009) 764.
[25] Maingi, R. T.H. Osborne, B.P. LeBlanc et al., Phys. Rev. Lett. **103** (2009) 075001.
[26] Maingi, R., R.E. Bell, J.M. Canik et al., Phys. Rev. Lett. **105** (2010) 135004.
[27] Boyle, D.P. R. Maingi, P.B. Snyder et al., Plasma Phys. Controlled Fusion **53** (2011) 105011.
[28] Boyle, D.P., J.M. Canik, R. Maingi et al., J. Nucl. Materials **438** (2013) S979.
[29] Canik, J.M., W. Guttenfelder, R. Maingi et al., Nucl. Fusion **53** (2013) 113016.
[30] Gray, T.K., J.M. Canik, R. Maingi et al., Nucl. Fusion **54** (2014) 043013.
[31] Ku, S., C.S. Chang and P.H. Diamond, Nucl. Fusion **49** (2009) 115021.
[32] Jaworski, M.A., A. Khodak, R. Kaita, Plasma Phys. Controlled Fusion **55** (2013) 124040.
[33] Kugel, H.W. et al., Fusion Eng. Design **85** (2010) 865.
[34] Podesta, M.A., R.E. Bell, A. Diallo et al., Nucl. Fusion **52** (2012) 037001.
[35] Scotti, F., V.A. Soukhanovskii, J.-W. Ahn et al., to be published in Journ. Nucl. Materials (2014).
[36] De Temmerman, G., et al., J. Vac. Sci. Technol. A **30** (2012) 041306.
[37] Wang, W.X. et al., Phys. Plasmas **17** (2010) 072511.
[38] Rebut, P.H. and M. Brusati, Plasma Phys. Controlled Fusion **28** (1986) 113.
[39] Rebut, P.H., P.P. Lallia and M.L. Watkins, The critical temperature gradient model of plasma transport: applications for JET and future tokamaks (Proc. 12th IAEA Conf. on Plasma Physics and Controlled Nuclear Fusion Research, Nice, France, 1988), 1988, IAEA-CN_50/D-4-1.
[40] Kaye, S.M., W. Guttenfelder, R.E. Bell, et al., Phys. Plasmas (2014).
[41] Podesta, M., M. Gorelenkova and R.B. White, Plasma Phys. Cont. Fusion **56** (2014) 055003.
[42] Cheng, C.Z. and M. Chance, J. Comput. Phys. **71** (1987) 124.
[43] Zhu, W., S.A. Sabbagh, R.E. Bell, et al., Phys. Rev. Lett. **96** (2006) 225002.
[44] Kim, K., J.-K. Park, A.H. Boozer, et al., Nucl. Fusion **54** (2014) 073014.
[45] Park, J.-K., A.H. Boozer and A.H. Glasser, Phys. Plasmas **14** (2007) 052110.
[46] Sun, Y., Y. Liang, K.C. Shaing, et al., Nucl. Fusion **51** (2011) 053015